phys. stat. sol. (a) **170**, 241 (1998)

Subject classification: 78.30.–j; 68.35.Ct; S5

First Experimental Results with the Free Electron Laser Coupled to a Scanning Near-Field Optical Microscope

A. CRICENTI[1]) (a), R. GENEROSI (a), C. BARCHESI (a), M. LUCE (a), M. RINALDI (a), C. COLUZZA (a), P. PERFETTI (a), G. MARGARITONDO (b), D. T. SCHAAFSMA (c), I. D. AGGARWAL (c), J. M. GILLIGAN (d), and N. H. TOLK (d)

(a) Istituto di Stuttura della Materia, via Fosso del Cavaliere 100, I-00133 Roma, Italy

(b) Institut de physique appliquée, Ecole Polytecnique Fédérale, CH-1015 Lausanne, Switzerland

(c) Optical Sciences Dvision, U.S. Naval Research Laboratory, 4555 Overlook Ave SE, Washington, DC 20375, USA

(d) Department of Physics and Astronomy, Vanderbilt University, Nashville, TN, USA

(Received June 18, 1998; in revised form September 23, 1998)

First experiments of coupling a free electron laser to a scanning near-field optical microscope (SNOM) are presented. To address the question of how important such spectroscopy can be for near-field infrared microscopy, we acquired images of the same region of the sample under investigation at several photon wavelengths. SNOM reflectivity images revealed features that were not present in the corresponding shear-force (topology) ones and which were due to localized changes in the bulk properties of the sample. Optical data in the infrared (near 3.5 μm), using the probe tips in collection mode, indicates an optical spatial resolution well below the classical limit of $\lambda/2$.

1. Introduction

We propose a combination of the spectroscopy with infrared radiation emitted by a free electron laser (FEL) and of a scanning near-field optical microscope (SNOM) [1 to 6] to investigate lateral variations in the bulk optical properties with lateral resolution well below the diffraction limit.

In the infrared region intramolecular modes exist, so this radiation region plays an important role in analytical work. This has applications to the fields of polymer chemistry, biology and material science, with particular application to semiconductors, whose gaps and band discontinuities lie in this region [7]. Furthermore, by the infrared radiation it is possible to excite electron phototransport across solid interfaces [8]: the accuracy of such measurements is sufficient to discriminate the different contributions to the transport processes and, due to the deep photon penetration, it can provide information on buried interfaces overcoming the limitation imposed by other experimental approaches, as photoemission spectroscopy.

[1]) Corresponding author.
Tel.: 39-6-49 93 41 43, Fax: 39-6-49 93 41 53, e-mail: antonio@dns.ism.rm.cnr.it

Unfortunately, many of the interface properties and of the chemical-physical processes suffer for strong spatial inhomogeneities [9]. This is an important point since spatial average over a large surface with non-uniformity in the properties, can introduce errors by broadening the experimental results due to the superposition of different local components. However, if the probe is spatially resolved, then maps can be made with contrast based on the local infrared activity. There are two ways to perform spatially resolved measurements: the scanning mode and the imaging mode. In the first method the exciting probe is focused on small area of the surface of the sample to be measured. In the second mode, the exciting source is shined over all the surface and the response signal is collected in such way to be spatially sensitive. The advantage of the scanning mode is that it does not demand a very flat sample, but, on the contrary, it is possible to create strong local non-equilibrium condition. In the case of semiconductor interfaces, this non-equilibrium process could induce artifacts in the experimental results, due, for example, to local band bending variations. The use of FEL radiation allows to illuminate the entire area of large samples and thus guarantes the homogeneity of the photon excitation. If the reflected signal is collected by a stretched optical fiber with a very small open edge aperture and in near-field condition, it is possible to perform spatially resolved measurements with lateral resolution well below the diffraction limit. The near-field condition is verified by the shear-force approach [10] that is able, also, to supply the local topology at the same time and on the same small area, from where we detect the optical signal. Using this approach, it is possible to reach a lateral resolution of few nanometers, as demonstrated by several works [11, 12]. The importance of this paper is determined by the potential applications of the technique and in general of the infrared free electron laser in buried interfaces and, more in general, in solid state research.

2. Experiment

Fig. 1 shows the experimental set-up. In the Vanderbilt free electron laser (FEL) the electron beam is produced by a 45 MeV radiofrequency accelerator, operating at a frequency of up to 2.856 Ghz. The source is tunable over the 2 to 10 μm wavelength range (first harmonic, down to 1 μm in third harmonic) with high output power and brightness. Pulses with 6 μs duration, 360 mJ energy, and 11 W average power (repetition rate 30 Hz) have been reliably demonstrated in tests conducted at the wavelength of 4.8 μm.

The apparatus for controlling the SNOM scanning unit, the data acquisition system and the image elaboration are fully described elsewhere [13 to 15]. To detect a shear force signal a 670 nm single-mode diode laser ($P = 1$ to 4 mW, LaserMax Inc.), equipped with a homemade front lens, producing a minimum spot size of 5 μm, is mounted on an adjustable plate with two spring-loaded stainless steel screws. The laser beam is focused onto the external body of the oscillating fiber that we used as scanning probe. The resulting shadow is revealed by a two-sector position sensitive detector [16] situated on the opposite side. The alternating signal is revealed by an AC/DC converter and fed into the electronic feedback loop to keep a constant shear-force signal between fiber and sample while scanning the sample. This system is different from the standard shear-force circuit [10], where a lock-in amplifier is used to detect the fiber oscillation signal. We tested both possibilities with our microscope: the AC/DC converter response was faster and much more stable and reliable, allowing several hours operation without

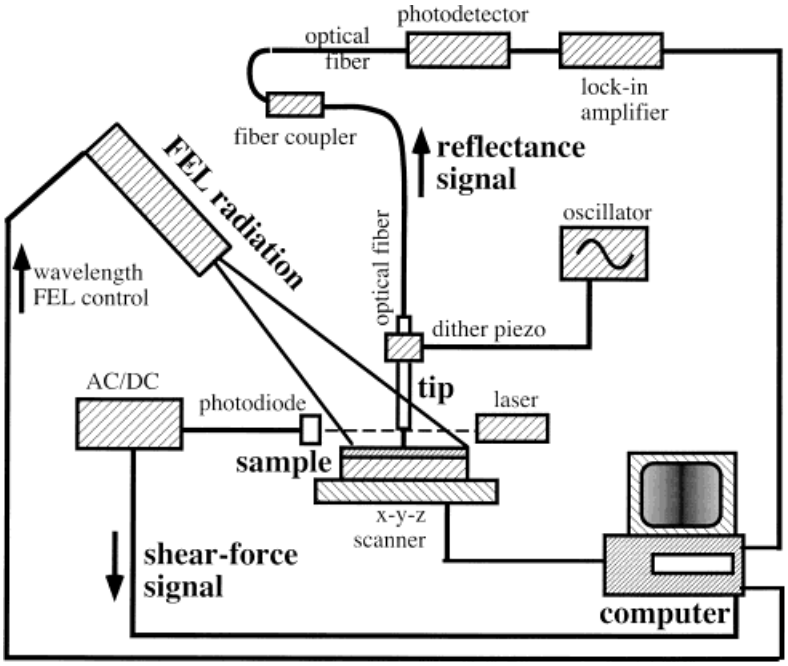

Fig. 1. Schematics of the experimental SNOM-FEL set-up

any mechanical adjustment. Shear-force images are taken with a signal that is 70% of the initial amplitude value of free oscillation.

The SNOM instrument allows to measure the reflectivity of the sample with the optical fiber when the sample is illuminated by an external source. The light picked up during the scanning through the fiber pin-hole, allows the mapping of the reflectivity of the sample. In order to detect the reflectivity signal a photodetector has been used. The detected signal is revealed by a lock-in amplifier whose analog output is converted by an ADC module and read by the computer through a digital I/O card. Topographical and optical images were taken simultaneously, with the FEL illuminating the specimen over a broad area and the SNOM probe collecting the reflected light. All the images shown are unfiltered, just a rigid plane subtraction is applied; brighter areas correspond to higher topography values (or to higher current in the optical image).

Infrared SNOM (IR-SNOM) probes were made from single-mode arsenic sulfide fiber (with outside diameter 80 to 140 μm and core approximately 10 μm), fabricated and tested at the Naval Research Laboratory. The tips were made using a standard micropipette puller (Sutter P-2000), with either a heated filament or an external visible laser used to soften the fiber. In addition, the 160 g static tension of the micropipette puller was often enough to break the thin-diameter chalcogenide fiber, so a counterbalance system had to be devised to relieve some of the static load.

3. Experimental Results

Several experiments have been performed: as representative examples we report on the measurements on a PtSi/Si sample and diamond grains on a silicon substrate. The PtSi/Si

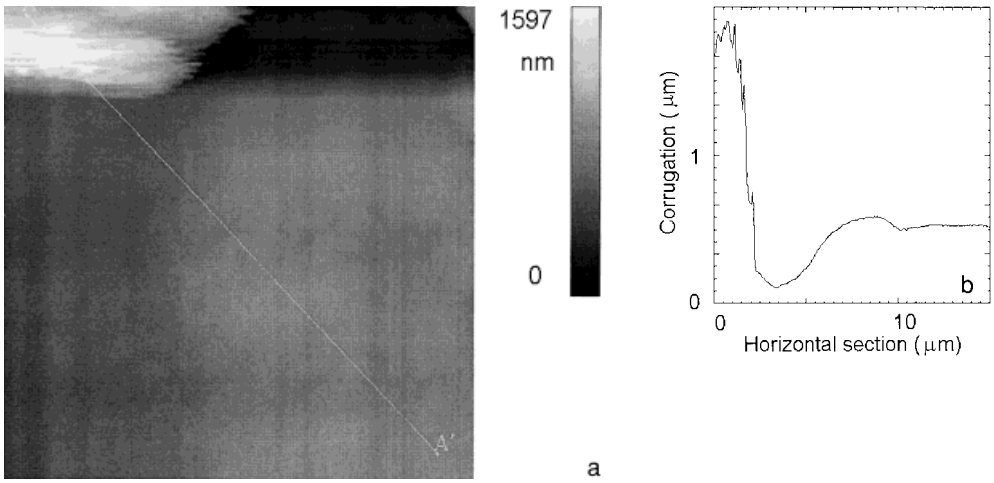

Fig. 2. a) Shear-force topography image ($12 \times 12\ \mu m^2$) of a PtSi/Si sample; b) corrugation along the AA′ line of Fig. 2a

samples were obtained by evaporation of 4 nm of Pt on a Si substrate held at room temperature. The sample was then ennealed at 350 °C in order to form a PtSi/Si interface. The substrates were cleaned prior to Pt evaporation by standard techniques. Fig. 2a is a $12 \times 12\ \mu m^2$ shear force-image taken on the PtSi/Si surface. In Fig. 2b we represent the corrugation of the AA′ line of Fig. 2a. A big structure (corrugation around 1500 nm) is present in the upper left corner. We point out that the appearance of the topology as measured by shear force are in general quite smooth with variation of several tens of nanometers. We choose this region since the above big structure was easily recognizable also in the optical images thus giving a good reference point. As visible, there is, in the center of the image, a round shape structure whose topographical corrugation is around 150 nm.

Fig. 3a is the reflectivity image of the same zone as in Fig. 2a, taken with a wavelength for the incident photons of 2.4 μm. The big structure, visible in Fig. 2a is present in the upper left corner and gives also here a clear contrast while a valley, 1000 nm wide (full width half maximum) and 0.2 mV amplitude, is crossing the image. It is important to stress the fact that such valley crosses the topographical structure in the center of Fig. 2a so that the two features are totally uncorrelated. The valley is also present in zones where there is no contribution in the topographical image, and, due to the deep penetration of the infrared light must be located well below the surface: it is, presumably, a Si groove. In this case, one can strongly consider that the near-field optical profile is purely optical and that the relief contrast of the sample surface has not taken part in the variation of the SNOM signal. Data (not shown here) have also been collected with 1.2 μm and 0.65 μm incident photon wavelength in the case of 1.2 μm the Si groove was still visible while it has disappeared when using 0.65 μm. This indicates that the "valley" in the 2.4 and 1.2 μm images is deeper than the maximum penetration of 0.63 μm photons.

In Fig. 3b we represent the corrugation of the AA′ line of Fig. 3a. From the smallest visible features, we estimated that the lateral resolution was better than 100 nm for topographic images, and than 200 to 400 nm for reflectivity images. These values are

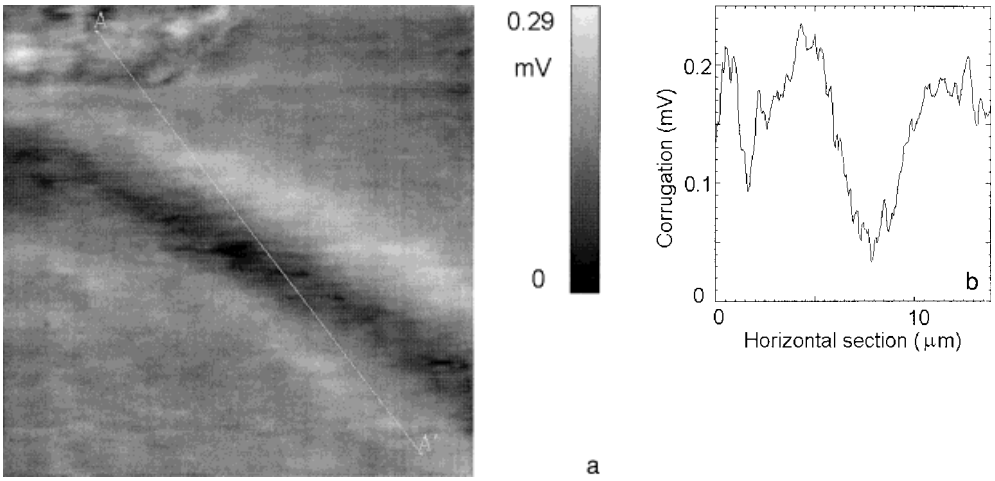

Fig. 3. a) Reflectivity image, taken simultaneously to the topography of Fig. 2a of a PtSi/Si sample taken with a photon of 2.4 μm; b) corrugation along the AA′ line of Fig. 3a

consistent with a much larger set of data not explicitly presented here and are better than the classical limit of $\lambda/2$.

The second specimen presented here is a polycrystalline diamond film prepared by vapor-phase deposition on a silicon substrate. Fig. 4a shows a $10 \times 10\,\mu m^2$ shear-force image while Fig. 4b shows the corrugation along the AA′ line. Small features on the individual diamond grains are quite well resolved: from reproducible structures in several consecutely acquired images we estimated the best lateral resolution of the probe to be between 50 and 80 nm. Since irregularities in the probe are expected to be a large detriment to lateral resolution on rough specimens these topographical images indicate that the probe tip itself was smoothly rounded.

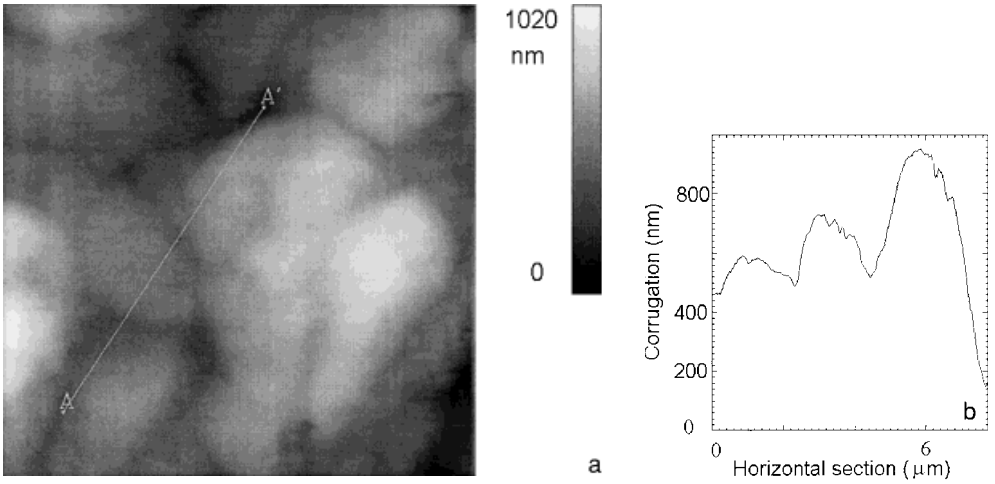

Fig. 4a. a) Shear-force topography image ($10 \times 10\,\mu m^2$) of diamond grains on a silicon substrate, b) corrugation along the AA′ line of Fig. 4a

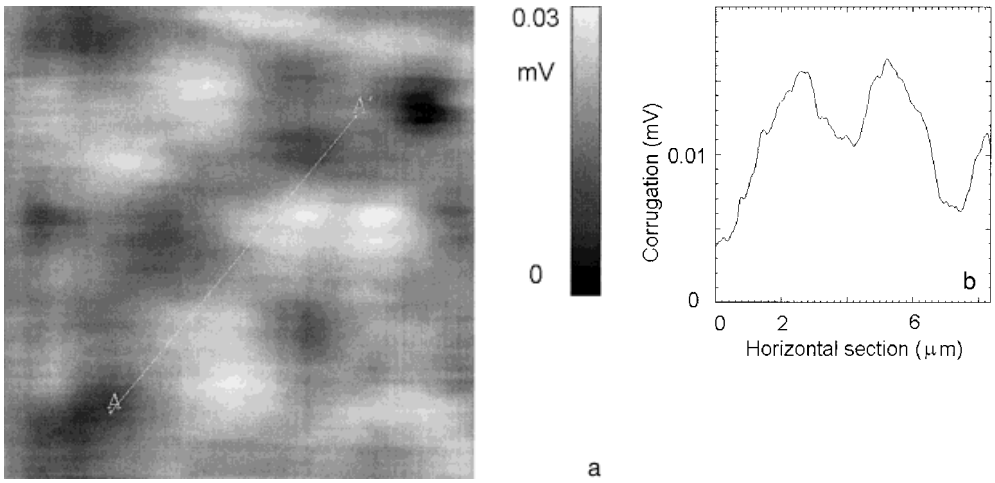

Fig. 5. a) Reflectivity image, taken simultaneously to the topography of Fig. 4a of diamond grains on a silicon substrate taken with a photon of 3.5 μm; b) corrugation along the AA′ line of Fig. 5a

Since the film had been annealed to remove residual hydrogen and water, it was of greatest interest in the optical experiment to look for absorption near 3.5 μm due to the C–H vibrational stretch mode. Fig. 5a shows a $10 \times 10\,\mu m^2$ reflectivity image of the same zone as in Fig. 4a, with the FEL operating at 3.5 μm. The correlation between optical data and certain features in the topographical image can be seen clearly. When the FEL was tuned outside the C–H absorption band (to 3.2 or 3.7 μm), the topographical image was reproduced, while the optical image became featureless, indicating that the dark regions in the optical image of Fig. 5a correspond to regions where the absorption was stronger, or where there was residual hydrogen in the film. In Fig. 5b we represent the corrugation of the AA′ line of Fig. 5a. Though the relative intensity noise in the FEL (which could not be normalized out in the apparatus used for this report) is evident in Fig. 5, several small features and edges are still resolved. From these, we estimated the optical lateral resolution to be well below the classical limit of $\lambda/2$.

In a recent paper [5] on reflection SNOM using uncoated optical fibers, there was shown a nearly one-to-one correspondence between the optical and topographical resolution. The authors reached the conclusion that dielectric tips have a limitation in lateral resolution of the order of $\lambda/2$. In our optical images (shown here and to appear in other papers) there is no correspondence with the topographic ones and a resolution well below the classical limit of $\lambda/2$ was achieved. The reason for such difference may lie in the different optical fibers and the different experimental set-up.

These results clearly indicate that the use of tunable infrared FEL radiation together with near-field optical collection open the way to realize a non-destructive tool able to measure buried properties of solid samples. The tunability of the source as well as the variation in the incident angle will allow a three-dimensional reconstruction of the shape and position of features and local inhomogeneities deeply located on the sample.

References

[1] D. W. Pohl, W. Denk, and M. Lanz, Appl. Phys. Lett. **44**, 651 (1984).
[2] E. Betzig, J. K. Trautman, T. D. Harris, J. S. Weiner, and R. L. Kostelak, Science **251**, 1468 (1991).
[3] D. Courjon and C. Bainier, Rep. Prog. Phys. **57**, 989 (1994).
[4] F. Zenhausern, Y. Martin, and H. K. Wickramasinghe, Science **269**, 1083 (1995).
[5] V. Sandoghdar, S. Wegscheider, G. Krausch, and J. Mlynek, J. Appl. Phys. **81**, 2499 (1997).
[6] M. Labardi, P. G. Gucciardi, M. Allegrini, and C. Pelosi, Appl. Phys. A **66**, S397 (1998).
[7] E. Yuncel et al., Phys. Rev. Lett. **70**, 4146 (1993).
[8] C. Coluzza et al., Phys. Rev. B **46**, 12834 (1992).
[9] G. Margaritondo, F. Gozzo, and C. Coluzza, Phys. Rev. B **47**, 9907 (1993).
[10] E. Betzig, P. L. Finn, and J. S. Wiener, Appl. Phys. Lett. **60**, 2484 (1994).
[11] D. W. Pohl and D. Courjon (Ed.), NATO ASI Series Near-Field Optics, Vol. 262, Kluwer Academic Press, 1992.
[12] J. Almeida et al., Appl. Phys. Lett. **69**, 2361 (1996).
[13] A. Cricenti and R. Generosi, Rev. Sci. Instrum. **66**, 2843 (1995).
[14] C. Barchesi, A. Cricenti, R. Generosi, C. Giammichele, M. Luce, and M. Rinaldi, Rev. Sci. Instrum. **68**, 3799 (1997).
[15] A. Cricenti, R. Generosi, C. Barchesi, M. Luce, and M. Rinaldi, Rev. Sci. Instrum. **69**, 3240 (1998).
[16] Spot segmented photodiodes, SPOT-4D, UDT Sensors Inc.